JOURNAL OF Materials CHEMISTRY

Crystal structure of a strontium–tantalum and a magnesium–niobium heterometal alkoxide: precursors for the MOCVD of ferroelectric oxides

Anthony C. Jones,*[a,c] Hywel O. Davies,*[a] Timothy J. Leedham,[a] Peter J. Wright,[b] Michael J. Crosbie,[b] Alexander Steiner,[c] Jamie F. Bickley,[c] Paul O'Brien,[d] Andrew J. P. White[d] and David J. Williams[d]

[a]*Inorgtech Limited, 25 James Carter Road, Mildenhall, Suffolk, UK IP28 7DE*
[b]*Defence Evaluation and Research Agency, St. Andrews Road, Malvern, Worcestershire, UK WR14 3PS*
[c]*Department of Chemistry, University of Liverpool, Liverpool, UK L69 7ZD*
[d]*Department of Chemistry, Imperial College of Science, Technology and Medicine, London, UK SW7 2AY*

Received 9th August 2000, Accepted 18th October 2000
First published as an Advance Article on the web 7th December 2000

The heterometal alkoxides $Sr[Ta(OPr^i)_6]_2{\cdot}2Pr^iOH$ **1** and $Mg[Nb(OEt)_6]_2{\cdot}2EtOH$ **2** have been structurally characterised by X-ray diffraction. Compound **1** is a precursor for the deposition of strontium bismuth tantalate ($SrBi_2Ta_2O_9$) by metalorganic chemical vapour deposition (MOCVD), whilst **2** is a potential precursor for the MOCVD of lead magnesium niobate [$Pb(Mg_{0.33}Nb_{0.66})O_3$]. In this paper it is shown how the presence of $Pb(thd)_2$ (thd = 2,2,6,6-tetramethylheptane-3,5-dionate) significantly influences the deposition chemistry of **2**. In the absence of $Pb(thd)_2$ and at low substrate temperatures (*ca.* 425 °C) the Mg : Nb ratio in the oxide film grown from **2** is close to 1 : 2, whereas at higher substrate temperatures (600 °C) the films are magnesium deficient, indicating partial decomposition of **2**. However, in the presence of $Pb(thd)_2$ films grown from **2** at low temperature (425–500 °C) contain no detectable Mg whilst the 1 : 2 Mg : Nb ratio, required in $Pb(Mg_{0.33}Nb_{0.66})O_3$, is now obtained at higher substrate temperatures (600 °C). This is attributed to the formation of a thermally stable Mg β-diketonate species *via* a gas-phase ligand exchange reaction between $Pb(thd)_2$ and **2**.

1 Introduction

Thin films of ferreoelectric metal oxides such as $(Ba,Sr)TiO_3$, $Pb(Zr,Ti)O_3$, $SrBi_2Ta_2O_9$ and $Pb(Mg,Nb)O_3$ have a variety of important applications in microelectronics and telecommunications, including next generation computer memories, infrared detectors and electro-optic storage.[1,2]

Ferroelectric thin films have been deposited by a number of techniques such as sol–gel deposition, sputtering, laser ablation and metalorganic chemical vapour deposition (MOCVD).[2,3] Of these techniques, MOCVD offers the most flexible approach, having the advantages of large area deposition capability, good composition control and high film uniformity, high deposition rates and excellent conformal step coverage on complex structures. An essential requirement for a successful MOCVD technology is the availability of suitable precursors with the appropriate physical characteristics and deposition behaviour.

The low vapour pressure of most oxide precursors (generally metal alkoxides or β-diketonates) requires high source temperatures of >200 °C to achieve viable deposition rates by conventional 'bubbler'-based MOCVD techniques, and this can lead to decomposition of the precursor with time. Consequently, liquid injection MOCVD, in which a solution of the precursor is injected directly into a heated evaporator is now widely used for the deposition of complex oxides.[4–6] This approach minimises thermal degradation of precursors but leads to the added requirement that the precursor must be stable for long periods in solution. Co-precursors should also evaporate at a common temperature, otherwise blockages will occur in the evaporator and reactor inlet pipes. Ideally, the separate precursors should also deposit oxide films in a similar temperature regime in order to achieve good layer uniformity. Therefore, a key element in the selection of precursors for liquid injection MOCVD is their compatibility in solution and in the gas phase.

Strontium bismuth tantalate, $SrBi_2Ta_2O_9$ (SBT) is a particularly important material, having major potential applications in non-volatile ferroelectric computer memories.[7] However, the liquid injection MOCVD of SBT has thus far been severely restricted by a lack of suitable precursors. Conventional precursors[8–10] include $Sr(thd)_2$ (where thd = 2,2,6,6-tetramethylheptane-3,5-dionate), $Bi(thd)_3$, $Bi(C_6H_5)_3$ and $Ta(OEt)_5$ and $Ta(OPr^i)_4(thd)$, and these are generally incompatible, having very different physical properties and decomposition characteristics. A potential solution to this problem is the use of 'single source' precursors, which contain two or more of the elements required in the oxide film in a single molecule, and the Sr–Ta double alkoxide $Sr[Ta(OPr^i)_6]_2$ has been investigated as a precursor to SBT.[11] More recently, $Sr[Ta(OEt)_5(dmae)]_2$ (dmaeH = 2-dimethylaminoethanol) has been used to deposit $SrTa_2O_6$[12] and SBT,[13] whilst $Sr[Ta(OEt)_6]_2$ has been used to deposit SBT.[14]

To date, $Sr[Ta(OEt)_5(bis\text{-}dmap)]_2$ [bis-dmapH = 1,3-bis(dimethylamino)propan-2-ol] is the only Sr–Ta double alkoxide which has been structurally characterised,[15] and in this paper we report the structure determination of $Sr[Ta(OPr^i)_6]_2{\cdot}2\text{-}Pr^iOH$.

The successful use of Sr–Ta alkoxides in MOCVD has encouraged us to extend the 'single source' approach to the

 DOI: 10.1039/b006529n

liquid injection MOCVD of lead magnesium niobate, $Pb(Mg_{0.33}Nb_{0.66})O_3$ (PMN), for which the conventional precursors $Pb(thd)_2$, $Mg(thd)_2$ and $Nb(OEt)_5$[16] also suffer from problems of incompatibility. In this paper, the structure of $Mg[Nb(OEt)_6]_2{\cdot}2EtOH$ is reported, together with preliminary data on its use in MOCVD.

2 Experimental

General techniques

Thermogravimetric analysis (TGA) was performed on a Shimadzu TGA 52 apparatus. The samples were held under an argon atmosphere and a heating rate of 20 °C min^{-1} was used. ^1H NMR spectra were obtained on a Bruker 300 NMR spectrometer and elemental microanalyses were carried out by the Chemistry Department service at Liverpool University. The composition of the films was determined using energy dispersive X-ray analysis (EDXA) or Auger electron spectroscopy (AES). An accelerating voltage of 20 kV was used for the EDXA analyses. The analysis was a spot analysis carried out on three spots (estimated error: 2%). The AES was combined with sequential argon-ion bombardment to provide information from the bulk of the film and compositions were determined using experimentally derived sensitivity factors based upon PbO, NbO_2 and MgO reference materials.

Precursor synthesis

$Sr[Ta(OPr^i)_6]_2{\cdot}2Pr^iOH$ **1** was synthesised according to the literature[17] by the addition of $Ta(OPr^i)_5$ (2 equiv.) to a solution of Sr metal in Pr^iOH solvent. $Mg[Nb(OEt)_6]_2{\cdot}2EtOH$ **2** was synthesised by addition of $Nb(OEt)_5$ (2 equiv.) to $Mg(OEt)_2$ in EtOH.[17] The identity of each compound was confirmed by proton NMR and elemental microanalysis.

$Sr[Ta(OPr^i)_6]_2{\cdot}2Pr^iOH$ (1). ^1H NMR ($CDCl_3$, 25 °C, 300 MHz) δ (ppm): 1.21 [s, 72 H, $OCH(CH_3)_2$], 1.22 [s, 12H, $HOCH(CH_3)_2$], 4.1 [br, 2H, $HOCH(CH_3)_2$], 4.64 [septet, 12H, $OCH(CH_3)_2$]. Anal. Found: C, 39.10; H, 7.50. Calc. for $C_{42}H_{98}O_{14}SrTa_2$: C, 39.48; H, 7.68%.

$Mg[Nb(OEt)_6]_2{\cdot}2EtOH$ (2). ^1H NMR (C_6D_6, 25 °C, 300 MHz) δ (ppm): 1.09 [t, 6 H, $HOCH_2CH_3$], 1.38 [t, 36 H, OCH_2CH_3], 3.55 [q, 4 H, $HOCH_2CH_3$], 3.93 [s, 2 H, $HOCH_2CH_3$], 4.43 (q, 24 H, OCH_2CH_3]. Anal. Found: C, 39.35; H, 8.45. Calc. for $C_{28}H_{72}O_{14}MgNb_2$: C, 39.85; H, 8.54%.

Single crystal X-ray diffraction

Crystals of **1** and **2** were obtained directly from the respective mother liquors. Selected crystals of **1** were mounted on a Siemens P4/RA diffractometer and crystals of **2** were mounted on an STOE-IPDS diffractometer, both using graphite monochromated Mo-Kα radiation ($\lambda = 0.71073$ Å, $T = 203$ K **1**, 293 K **2**). The structures were solved by direct methods and were refined by full matrix least squares based on F^2. Hydrogen atoms were placed in calculated positions and allowed to ride on the parent atom. Computations on **1** were carried out using the SHELXTL program[18] and SHELX97[19] on **2**. Lattice parameters and basic information on data collection are summarised in Table 1.

CCDC 1145/258. See http://www.rsc.org/suppdata/jm/b0/b006529n/ for crystallographic files in .cif format.

MOCVD

Thin films of magnesium niobium oxide and PMN were deposited on silicon substrates by liquid injection MOCVD using solutions of **2** in tetrahydrofuran (THF) or a single THF solution containing both **2** and $Pb(thd)_2$ (Inorgtech). The films were deposited onto Si(100) substrates over a range of temperatures from 425 to 600 °C using a hot wall MOCVD reactor described elsewhere.[6] The films were grown (Table 2) at various substrate temperatures and deposition times were varied (from 1 to 4 h) to obtain films of adequate thickness for analysis (>200 nm). Film thickness was determined by scanning electron microscopy and by weight. (Values agreed to within 5%.) The magnesium niobium oxide and PMN thin films were adhesive (Scotch tape test) and conformal over the edges of the substrate, and displayed uniformity better than +/− 5% over a 2 cm × 2 cm wafer (typically +/−2% within the central 1 cm^2).

Table 1 Crystal and data collection parameters for **1** and **2**

Empirical formula	$C_{42}H_{98}O_{14}SrTa_2$ **1**	$C_{28}H_{72}O_{14}MgNb_2$ **2**
Formula weight	1276.72	843.13
a/Å	10.851(4)	8.956(3)
b/Å	14.492(5)	11.370(3)
c/Å	19.113(7)	11.630(5)
α/°	97.43(3)	95.79(4)
β/°	96.38(4)	110.06(4)
γ/°	102.84(3)	94.27(4)
V /Å^3	2875(2)	1099.2(6)
Crystal system	Triclinic	Triclinic
Space group	$P\bar{1}$ (no. 2)	$P\bar{1}$
Z	2	1
Absorption coefficient	4.772 mm^{-1}	0.511 mm^{-1}
Reflections collected	7893	6878
Reflections unique (R_{int})	7417 (0.0582)	3199 (0.0517)
$R1$ [$I > 2\sigma(I)$]	0.0473	0.0478
$wR2$ (all data)	0.1130	0.1366

3 Results and discussion

Crystal structure of 1

The crystal structure of **1** is shown in Fig. 1 and selected bond distances and angles are given in Table 3. The compound is composed of discrete trinuclear units containing a six-coordinate strontium and two six-coordinate tantalum atoms, each displaying distorted octahedral symmetry. The coordination around the strontium atom is completed by two adducting ethanol ligands in the *cis* position. The terminal Ta–O bonds are shorter [1.889(8)–1.915(8) Å] than the Ta–O bonds involved in μ-bridging to Ta [2.009(8)–2.046(6) Å], whilst the axial Ta–O bonds lie in an intermediate range [1.886(8)–2.017(7) Å]. The Ta–O bond bond distances in **1** are similar to those in the only other structurally characterised Sr–Ta double metal alkoxide, $Sr[Ta(OEt)_5(bis\text{-}dmap)]_2$ [terminal Ta–O: 1.870(11)–1.906(11) Å; bridging Ta–O: 1.983(9)–2.032(9) Å].[15] However, the non-bonded Sr···Ta separation Sr–Ta in **1** of 3.71 Å is significantly longer than the Sr-Ta distance in $Sr[Ta(OEt)_5(bis\text{-}dmap)]_2$ (3.41 Å), indicating that the donor functionalised bis-dmap ligand has increased the interaction between the Sr and Ta centres. The Sr–O bond distances in **1** [2.519(8)–2.554(8) Å] are similar to those in $Sr[Ta(OEt)_5(bis\text{-}dmap)]_2$ [2.547(8)–2.669(8) Å] and there is no significant

Table 2 Growth conditions used to deposit $MgNb_2O_6$[a] and PMN[b] by liquid injection MOCVD using **1** and $Pb(thd)_2$

Reactor pressure	20 mbar
Substrates	Si(100)
Precursor solution injection rate	3–5 $cm^3\ h^{-1}$
Argon flow rate	4000 $cm^3\ min^{-1}$
Oxygen flow rate	1000 $cm^3\ h^{-1}$
Evaporator temperature	225 °C
Substrate temperature	300–600 °C

[a]0.1 molar solution of **2** in THF. [b]50% 0.1 molar THF solution of **2**/50% 0.2 molar THF solution of $Pb(thd)_2$.

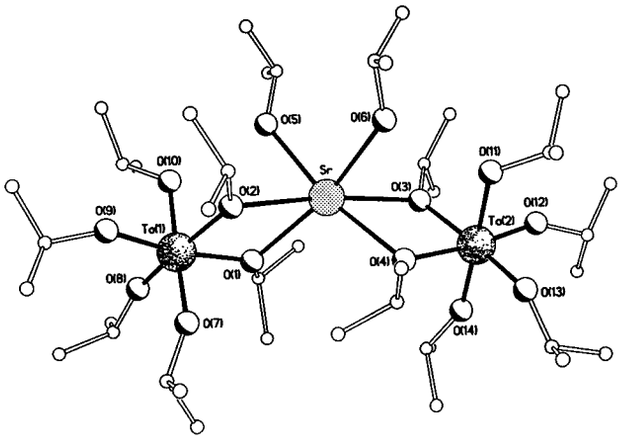

Fig. 1 Crystal structure of $Sr[Ta(OPr^i)_6]_2 \cdot 2Pr^iOH$ **1**.

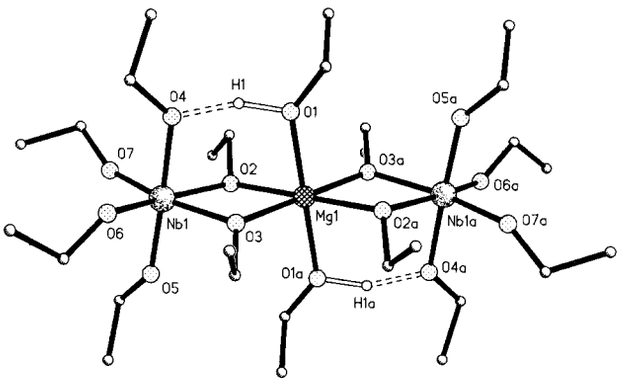

Fig. 2 Crystal structure of $Mg[Nb(OEt)_6]_2 \cdot 2EtOH$ **2**.

difference between the adducting EtOH Sr–O bond length and the bridging alkoxide Sr–O bond distances.

The terminal O–Ta–O bond angles (95.1, 95.2°) are significantly larger than the angles of 79.7(3), 78.7(3)° subtended by the O–Ta–O bonds involved in bridging to Sr, leading to a highly distorted octahedral configuration of oxygen atoms around the Ta centres. Similarly, the O–Sr–O angles are distorted from 90°, with values ranging from 61.3 to 111.3°.

Crystal structure of 2

In the crystalline state **2** consists of discrete trinuclear molecules which have a two-fold axis through the central Mg atom (Fig. 2). The Nb and Mg atoms are six-coordinate, and in the case of Mg this coordination is achieved by the addition of two *trans* adducting EtOH ligands. The hydrogen atom on each of these EtOH ligands forms an intramolecular bond [distance 2.681(5) Å] with the oxygen atom of two axial [OEt] groups on adjacent Nb centres. The geometry around the Nb and Mg atoms is distorted octahedral. Only one other Mg/Nb double metal alkoxide has been structurally characterised, $Mg[Nb(OPr^i)_5(OAc)]_2$,[20] and this displays similar six-coordinate distorted octahedral geometries around the Mg and Nb atoms.

Selected bond distances and angles are given in Table 4. The structure of **2** is similar to that of $Mg[Nb(OPr^i)_5(OAc)]_2$, although the Nb–Mg–Nb angle of 180° in **2** is considerably larger than that in $Mg[Nb(OPr^i)_5(OAc)]_2$ (139°),[20] and the non-bonded Mg···Nb distance of 3.3273(2) Å in **2** is also slightly longer than that in $Mg[Nb(OPr^i)_5(OAc)]_2$ [3.194(3) Å]. The terminal equatorial Nb–O bonds in **2** are shorter [1.887(4) Å] than the Nb–O bonds involved in μ-bridging with the Mg [2.044(3) Å]. The axial Nb–O bond not involved in hydrogen bonding is slightly longer [1.903(4) Å] than the terminal Nb–O bonds, and intramolecular hydrogen bonding leads to an extension in the axial Nb–O bond length [1.995(3) Å]. The Nb–O bond distances in **2** span a range of 1.887(4)–2.058(3) Å, similar to the range observed in $Mg[Nb(OPr^i)_5(OAc)]_2$ [1.872(8)–2.175(6) Å],[20] and in $LiNb(OEt)_6$ [terminal Nb–O: 1.88(2)–1.98(1) Å][21] in which a similar trend in bond distances was observed [Nb–OR (terminal) distance < Nb–μ-OR (bridging) distance]. The short terminal Nb–O bond distances in **2**, $Mg[Nb(OPr^i)_5(OAc)]_2$ and $LiNb(OEt)_6$ can be attributed to the bonds having a significant π-character, characteristic of the early transition metals.[22]

The equatorial O–Nb–O bond angles all deviate significantly from 90°. The O–Nb–O bonds involved in bridging with Mg are significantly more acute at only 74.35(13)°, whilst the adjacent O–Nb–O bond angles are close to 90° [92.96(16)°, 93.20(16)°]. This leads to an opening out of the terminal O–Nb–O bond angle [99.25(19)°].

MOCVD of $MgNb_2O_6$ and PMN

The single source precursor **2** was used successfully to deposit thin films of magnesium niobium oxide. The composition of the films was determined by energy dispersive X-ray analysis (EDXA) (see Table 5) and X-ray diffraction (XRD).

Table 3 Selected bond distances (Å) and angles (°) in $Sr[Ta(OPr^i)_6]_2 \cdot 2Pr^iOH$ **1**

Ta(1)–O(9)	1.898(8)	Sr–O(2)	2.531(7)
Ta(1)–O(8)	1.889(8)	Sr–O(1)	2.519(8)
Ta(1)–O(7)	1.886(8)	Sr–O(5)	2.554(8)
Ta(1)–O(10)	2.014(8)	Sr–O(6)	2.535(9)
Ta(1)–O(2)	2.017(7)	Sr–O(3)	2.539(8)
Ta(1)–O(1)	2.046(6)	Sr–O(4)	2.478(8)
Ta(2)–O(12)	1.913(7)	Sr–Ta	3.41
Ta(2)–O(13)	1.915(8)		
Ta(2)–O(14)	1.915(7)		
Ta(2)–O(11)	2.017(7)		
Ta(2)–O(3)	2.009(8)		
Ta(2)–O(4)	2.027(7)		
O(8)–Ta(1)–O(9)	95.1(4)	O(1)–Sr–O(2)	62.1(2)
O(1)–Ta(1)–O(2)	79.7(3)	O(1)–Sr–O(4)	108.2(2)
O(1)–Ta(1)–O(10)	85.1(3)	O(4)–Sr–O(3)	61.3(2)
O(8)–Ta(1)–O(1)	91.8(3)	O(2)–Sr–O(3)	172.4(2)
O(9)–Ta(1)–O(2)	93.0(3)	O(2)–Sr–O(5)	78.1(3)
O(8)–Ta(1)–O(7)	93.2(4)	O(3)–Sr–O(6)	78.0(3)
O(8)–Ta(1)–O(10)	87.1(4)	O(5)–Sr–O(6)	93.4(3)
		O(2)–Sr–O(4)	111.3(2)
		O(5)–Sr–O(3)	109.4(3)
O(13)–Ta(2)–O(12)	95.2(4)		
O(4)–Ta(2)–O(3)	78.7(3)		
O(4)–Ta(2)–O(11)	87.5(3)		
O(4)–Ta(2)–O(13)	92.0(3)		
O(12)–Ta(2)–O(3)	93.9(4)		
O(13)–Ta(2)–O(14)	91.6(4)		
O(13)–Ta(2)–O(11)	88.6(4)		

Table 4 Selected bond distances (Å) and angles (°) in $Mg[Nb(OEt)_6]_2 \cdot 2EtOH$ **2**

Nb(1)–O(7)	1.887(4)	Mg–O(2)	2.061(3)
Nb(1)–O(6)	1.895(4)	Mg–O(3)	2.063(3)
Nb(1)–O(5)	1.903(4)	Mg–O(1)	2.092(3)
Nb(1)–O(4)	1.995(3)		
Nb(1)–O(2)	2.058(3)	H(1)–O(4)	2.681(5)
Nb(1)–O(3)	2.044(3)		
Mg–Nb	3.3273(2)		
O(6)–Nb(1)–O(7)	99.25(19)	O(3)–Mg–O(2)	73.89(13)
O(3)–Nb(1)–O(2)	74.35(13)	O(3)–Mg–O(2a)	106.11(13)
O(3)–Nb(1)–O(4)	87.99(14)	O(3)–Mg–O(1)	86.38(15)
O(6)–Nb(1)–O(3)	92.96(16)		
O(7)–Nb(1)–O(2)	93.20(16)	Nb(1)–Mg–Nb(2)	179.99(1)
O(6)–Nb(1)–O(5)	91.51(19)		
O(6)–Nb(1)–O(4)	87.29(17)		
O(5)–Nb(1)–O(3)	93.42(16)		

The EDXA data show that the composition of magnesium niobium oxide films, and in particular, the Mg : Nb ratio, is strongly dependent on substrate temperature. At low substrate temperatures (<450 °C), the Mg : Nb ratio is close to 1 : 2. However, the layers become Mg deficient on raising the substrate temperature. This strongly suggests that **2** is decomposing in the hot zone of the reactor in the presence of oxygen. At higher substrate temperatures, the temperature of the walls of the reactor approach the substrate temperature and at these temperatures it is probable that the adducting EtOH ligands will dissociate to leave an unsaturated four-coordinate Mg centre which will be highly susceptible to attack by oxygen. This will lead to pre-deposition of MgO upstream from the substrate, and to an increased concentration of the volatile $Nb(OEt)_5$ precursor in the gas phase. This in turn leads to an excess of Nb_2O_5 in the deposited oxide films.

XRD analysis on the magnesium niobium oxide films showed evidence of some single phase material when the Mg : Nb ratio was close to 1 : 2, but showed additional diffraction peaks due to niobium oxide when excess niobium was present in the films.

The growth rate of magnesium niobium oxide as a function of substrate temperature is shown in Fig. 3. The maximum growth rate occurs at approx. 475–525 °C, much higher than the optimum oxide deposition temperature from $Sr[Ta(OEt)_5(dmae)]_2$ (360 °C).[12] At substrate temperatures greater than 500 °C the growth rate of magnesium niobium oxide falls away rapidly due to thermal decomposition of the complex on the hot walls of the reactor.

TGA data, shown in Fig. 4(a), provide further evidence for the thermal decomposition of **2** with three separate regions of weight loss in evidence. The lower temperature region (20–250 °C) can be attributed to loss of the weakly adducting EtOH ligands, whilst the second and third regions of weight loss (250–325 and 325–400 °C) may correspond to the decomposition of the complex into its $Nb(OEt)_5$ and $Mg(OEt)_2$ components. TGA data for $Pb(thd)_2$ [Fig. 4(b)] show that it also evaporates in the 200–320 °C region indicating that the volatilities of **2** and $Pb(thd)_2$ are well matched for liquid injection applications. The evaporation behaviour of **2** contrasts with TGA data for $Sr[Ta(OEt)_5(dmae)]_2$ which evaporates cleanly in a single stage over the temperature range 200–330 °C.[23]

The addition of $Pb(thd)_2$ to the system significantly alters the deposition chemistry of **2**. The films were grown in the presence of a considerable excess of Pb, and EDXA data (see Table 6) indicate that, in marked contrast to growth using **2** alone, there was no incorporation of Mg at low substrate temperatures (425–500 °C). However, a Mg : Nb ratio of 1 : 2 in the oxide films was obtained at higher substrate temperatures (550–600 °C), irrespective of the concentration of Pb in the films. This is a significant result as it indicates that the use of **2** in combination with $Pb(thd)_2$ gives the 1 : 2 Mg : Nb ratio required in $Pb(Mg_{0.33}Nb_{0.66})O_3$ at growth temperatures of between 550 and 600 °C, which are precisely the temperatures favouring formation of the required perovskite phase of PMN.

Diffraction peaks attributable to both the pyrochlore and perovskite phases were detected in the XRD spectra of the PMN films, together with additional lines arising from PbO and niobium oxide. Low temperature deposition favoured the formation of the pyrochlore phase, whilst higher growth temperatures led to an increase in the perovskite phase. Further analysis of the PMN films by AES indicated that carbon was essentially absent (AES detection limit *ca.* 1 at%) from the bulk of the films.

The mechanism by which $Pb(thd)_2$ influences the decomposition behaviour of **2** has not been established. However, the deposition results from **2** alone (*i.e.* loss of Mg, increased Nb concentration in films) suggest that the precursor decomposes at temperatures above 425 °C. It is also known that $Pb(thd)_2$ starts to decompose at evaporator temperatures in the order of 250 °C and deposits oxide most efficiently in the range 450–500 °C.[24] Therefore at substrate temperatures of 550–600 °C, both **2** and $Pb(thd)_2$ are likely to decompose to some extent in the gas phase in the vicinity of the substrate and hot reactor walls. This may lead to interaction between liberated [thd^-] ligands, and the very oxygen-sensitive four-coordinate Mg centre in **2**. This in turn may lead to the formation of [Mg–thd] species [*e.g.* $Mg(thd)_2$ or (OEt)Mg(thd)], which have a relatively high thermal stability, leading to a deficiency of Mg in the oxide films at low substrate temperatures and more efficient incorporation of Mg at higher temperatures.

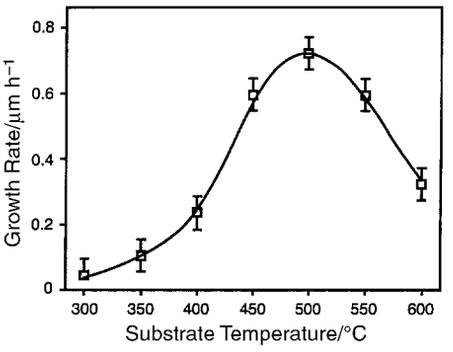

Fig. 3 Variation in growth rate of magnesium niobium oxide with substrate temperature.

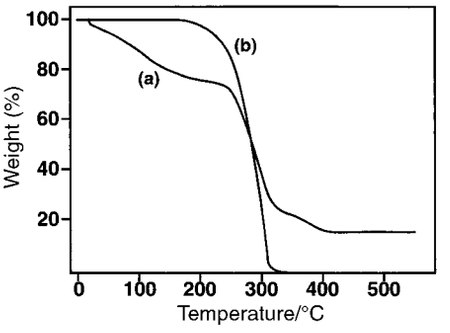

Fig. 4 TGA data for (a) $Mg[Nb(OEt)_6]_2{\cdot}2EtOH$ and (b) $Pb(thd)_2$.

Table 5 Composition of magnesium niobium oxide thin films determined by EDXA

	Composition (at%)			
Substrate temperature /°C	Mg	Nb	O	Mg : Nb
400	17.0	21.0	62.0	1 : 1.2
450	5.9	28.0	66.1	1 : 4.7
500	4.6	28.1	67.3	1 : 6.0
550	3.9	28.0	68.1	1 : 7.2
600	2.9	29.4	67.7	1 : 10

Table 6 EDXA data for lead magnesium niobate films deposited from $Mg[Nb(OEt)_6]_2{\cdot}2EtOH$ and $Pb(thd)_2$[a]

	Composition (at%)				
Substrate temperature /°C	Pb	Mg	Nb	O	Mg : Nb
425	54.9	ND	5.4	39.7	—
500	53.8	ND	5.5	40.7	—
550	48.8	2.4	6.5	42.3	1 : 2.6
600	48.9	3.8	7.8	39.5	1 : 2.0

[a]50% 0.1 M THF solution of $Mg[Nb(OEt)_6]_2{\cdot}2EtOH$/50% 0.2 M THF solution of $Pb(thd)_2$.

4 Conclusions

The structures of $Sr[Ta(OPr^i)_6]_2 \cdot 2Pr^iOH$ **1** and $Mg[Nb(OEt)_6]_2 \cdot 2EtOH$ **2** have been determined. Both compounds can be used as single source precursors for the growth of ferroelectric metal oxides by liquid injection MOCVD. However, the concentration of Mg in films grown using **2** is a strong function of substrate temperature. This suggests that **2** decomposes in the gas phase and then undergoes a ligand exchange reaction with $Pb(thd)_2$ to generate a more thermally stable Mg β-diketonate species.

Acknowledgements

We are grateful to G. W. Critchlow for providing AES data. We also acknowledge the support of the Teaching Company Directorate (H. O. D. was a Teaching Company Associate). P. O. B. was Sumitomo/STS Professor of Materials Chemistry.

References

1 Electroceramic Thin Films, Parts I and II, *MRS Bull.*, 1996, **21** and references therein.
2 Proc. 1st European Meeting on Integrated Ferroelectrics, eds. S. Namba, J. Kelly and M Van Rossum, *Microelectron. Eng.*, 1995, **29** and references therein.
3 Ferroelectric Thin Films IV, eds. B. A. Tuttle, S. B. Desu, R. Ramesh and T. Shiosaki, *Mater. Res. Soc. Symp. Proc.*, 1995, **361** and references therein.
4 F. Felten, J. P. Senateur, F. Weiss, R. Madar and A. Abrutius, *J. Phys. IV*, 1995, **5**, C5–1079.
5 I.-S. Chen, J. F. Roeder, T. E. Glassman and T. H. Baum, *Chem. Mater.*, 1999, **11**, 209.
6 A. C. Jones, T. J. Leedham, P. J. Wright, M. J. Crosbie, P. A. Lane, D. J. Williams, K. A. Fleeting, D. J. Otway and P. O'Brien, *Chem. Vap. Deposition*, 1998, **4**, 46.
7 C. A. Paz de Araujo, J. D. Cuchiaro, K. D. McMillan, M. C. Scott and J. F. Scott, *Nature*, 1995, **347**, 627.
8 T. Ami, K. Hironaka, C. Isobe, N. Nagl, M. Sugiyama, Y. Ikeda, K. Watanabe, A. Machida, K. Miura and M. Tanaka, *Mater. Res. Soc. Symp. Proc.*, 1996, **415**, 195.
9 T. Li, S. B. Desu, C. H. Peng and M. Nagata, *Appl. Phys. Lett.*, 1996, **68**, 616.
10 T. Li, Y. Zhu, S. B. Desu and M. Nagata, *Mater. Res. Soc. Symp. Proc.*, 1996, **415**, 189.
11 Y. Kojima, H. Kodakura, Y. Pkahara, M. Matsumoto and T. Mogi, *Int. Ferroelectrics*, 1997, **18**, 183.
12 M. J. Crosbie, P. J. Wright, H. O. Davies, A. C. Jones, T. J. Leedham, P. O'Brien and G. W. Critchlow, *Chem. Vap. Deposition*, 1999, **5**, 9.
13 S. Narayan, L. McMillan, C. Paz de Araujo, F. Schienle, D. Burgess, J. Lindner, M. Schumacher, H. Juergensen, K. Uchiyama and T. Otsuki, Paper No. 064 C, presented at 12th Int. Symp. on Integrated Ferroelectrics, March 12–15, 2000, Aachen, Germany.
14 H. Funakubo, N. Nukaga, K. Ishikawa and T. Watanabe, *Jpn. J. Appl. Phys.*, 1999, **38**, L199.
15 H. O. Davies, A. C. Jones, T. J. Leedham, P. O'Brien, A. J. P. White and D. J. Williams, *J. Mater. Chem.*, 1998, **8**, 2315.
16 S. Stemmer, G. R. Bai, N. D. Browning and S. K. Streiffer, *J. Appl. Phys.*, 2000, **87**, 3526.
17 S. Govil, P. N. Kapoor and R. C. Mehrotra, *J. Inorg. Nucl. Chem.*, 1976, **38**, 172.
18 Siemens SHELXTL PC Version 5.03, Siemens Analytical X-Ray Instruments Inc., Madison, WI, 1994.
19 G. M. Sheldrick, SHELX97 Program for crystal structure refinement, University of Göttingen, Germany, 1997.
20 S. Boulmaaz, R. Papiernik, L. G. Hubert-Pfalzgraf, B. Septe and J. Vaisserman, *J. Mater. Chem.*, 1997, **7**, 2053.
21 D. J. Eichorst, D. A. Payne and S. R. Wilson, *Inorg. Chem.*, 1990, **29**, 1458.
22 M. H. Chisholm, *Chemtracts: Inorg. Chem.*, 1992, **4**, 273.
23 H. O. Davies, T. J. Leedham and A. C. Jones, Inorgtech Limited, unpublished data, 1999.
24 A. C. Jones, T. J. Leedham, P. J. Wright, M. J. Crosbie, D. J. Williams, P. A. Lane and P. O'Brien, *Mater. Res. Soc. Symp. Proc.*, 1998, **495**, 11.